
An Adaptive Collocation Point Strategy For Physics Informed Neural Networks via the QR Discrete Empirical Interpolation Method

Adrian Celaya^{1,2} David Fuentes² Beatrice Riviere¹

Abstract

Physics-informed neural networks (PINNs) have gained significant attention for solving forward and inverse problems related to partial differential equations (PDEs). While advancements in loss functions and network architectures have improved PINN accuracy, the impact of collocation point sampling on their performance remains underexplored. Fixed sampling methods, such as uniform random sampling and equispaced grids, can fail to capture critical regions with high solution gradients, limiting their effectiveness for complex PDEs. Adaptive methods, inspired by adaptive mesh refinement from traditional numerical methods, address this by dynamically updating collocation points during training but may overlook residual dynamics between updates, potentially losing valuable information. To overcome this limitation, we propose an adaptive collocation point selection strategy utilizing the QR Discrete Empirical Interpolation Method (QR-DEIM), a reduced-order modeling technique for efficiently approximating nonlinear functions. Our results on benchmark PDEs, including the wave, Allen-Cahn, and Burgers' equations, demonstrate that our QR-DEIM-based approach improves PINN accuracy compared to existing methods, offering a promising direction for adaptive collocation point strategies.

(PDEs) (Karniadakis et al., 2021; Lu et al., 2021a; Raissi et al., 2019). By embedding the governing PDEs directly into the neural network's loss function via automatic differentiation, PINNs provide a flexible, mesh-free alternative to traditional numerical PDE solvers like the finite difference and finite element methods. Moreover, PINNs can easily incorporate physics-based constraints and observational data into loss functions. Applications of PINNs span a diverse range of areas in computational science and engineering, including computational fluid dynamics (Cai et al., 2021), coupled or multi-physics problems (Wang et al., 2023; Degen et al., 2022), and parameter estimation in biological systems (Yazdani et al., 2020).

Despite their successes, tackling increasingly complex problems with PINNs poses both theoretical and practical challenges (Wu et al., 2023). Since their introduction in (Raissi et al., 2019), numerous extensions of the original PINN framework have enhanced their computational performance and accuracy. For instance, meta-learning has led to the development of improved loss functions for PINNs (Psaros et al., 2022), while gradient-enhanced PINNs effectively integrate information about the PDE residual's gradient into their loss function (Yu et al., 2022). In addition to improved loss functions, recent developments have improved network architectures for PINNs. For instance, (Wang & Zhong, 2024) uses neural architecture search to find optimal neural network architectures for solving certain PDEs, and (Lu et al., 2021b) proposes networks that directly encode constraints like Dirichlet and periodic boundary conditions into the architecture.

PINNs minimize their loss function on a set of collocation points sampled from the problem's computational domain. The effect of these collocation points is similar to that of mesh or grid points in traditional numerical methods for PDEs. Therefore, the distribution of these points is crucial to the accuracy of PINNs. However, despite all of the recent advancements in loss functions and network architectures for PINNs, most of these methods tend to use simple collocation point sampling methods like uniformly sampling random points or an equispaced grid and do not consider the effect of collocation point sampling on their accuracy.

1. Introduction

In recent years, physics-informed neural networks (PINNs) have emerged as a powerful tool for solving forward and inverse problems involving partial differential equations

¹Department of Computational Applied Mathematics and Operations Research, Rice University, Houston, TX, USA ²Department of Imaging Physics, The University of Texas MD Anderson Cancer Center, Houston, TX, USA. Correspondence to: Adrian Celaya <acelaya@rice.edu>.

1.1. Previous Work

Collocation point sampling methods can be broadly classified into two categories: fixed and adaptive. As the name suggests, fixed methods generate a set of collocation points that remain constant throughout the training process. For instance, we could use points arranged in an equispaced grid or random samples drawn from a uniform distribution over the computational domain as collocation points. While these two approaches are widespread, other fixed methods include sampling from Latin hypercubes (Raissi et al., 2019), Sobol sequences (Pang et al., 2019), and Hammersley sequences (Wu et al., 2023).

An advantage of fixed sampling methods is their simplicity - they are trivial to implement and easy to use with training PINNs. However, they do not incorporate information about the residual during training and, as a result, can miss or undersample regions that contribute most to the overall error. For example, suppose the function $u(x, y) = 0.0005x^2(x-1)^2y^2(y-1)^2 \exp(10x^2 + 10y)$ is the solution to some PDE that we want to solve using a PINN where we sample collocation points with uniform random sampling on the domain $[0, 1] \times [0, 1]$. Figure 1 displays the solution u with the randomly sampled collocation points shown as red dots. The distribution of the collocation points highlights a common issue with fixed sampling methods: most points are in flat regions, while areas with high gradients in u are undersampled. This imbalance can negatively impact the accuracy of PINNs.

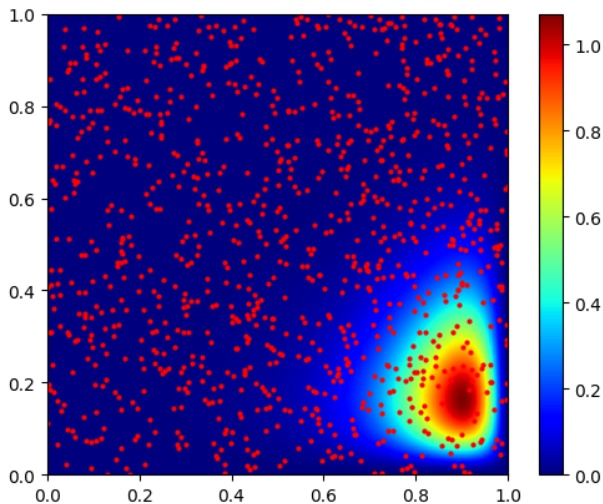


Figure 1. Visualization of $u(x, y) = 0.0005x^2(x-1)^2y^2(y-1)^2 \exp(10x^2 + 10y)$ with randomly sampled collocation points shown as red dots.

While fixed sampling methods work well for simple PDEs, they may not be sufficient for more complex problems. Inspired by adaptive mesh refinement in finite element meth-

ods, (Lu et al., 2021a) introduced the residual-based adaptive refinement method, which adds new residual points in locations with large PDE residuals - improving the accuracy of their PINN versus training with fixed sampling methods. Since its introduction, other versions of this greedy algorithm have been proposed in (Zeng et al., 2022; Hanna et al., 2022; Wu et al., 2023). Another approach for adaptive refinement is to construct a probability density function (PDF) based on the PDE residual and sample points according to this PDF. This method of sampling from a PDF instead of the points with the highest residual was first proposed in (Nabian et al., 2021), with similar approaches being investigated in (Wu et al., 2023; Zapf et al., 2022; Gao & Wang, 2023).

A common aspect of the adaptive methods mentioned above is that they sample collocation points at fixed iteration intervals from a large set of points that is separate from the training set. As a result, these methods do not directly consider the dynamics of the residuals between these intervals, which may lead to a loss of valuable information that could enhance the convergence of the training process and produce more accurate results. To address this issue, we propose an adaptive collocation point selection strategy that employs tools from reduced-order modeling (ROM) to directly incorporate these residual dynamics into the training of PINNs for solving forward problems related to PDEs. Specifically, we turn to the QR Discrete Empirical Interpolation Method (QR-DEIM), a common technique in ROM for efficiently approximating nonlinear functions (Chaturantabut & Sorensen, 2010; Drmac & Gugercin, 2016).

To the best of our knowledge, the first application of the QR-DEIM algorithm in relation to PINNs was proposed by Forootani et al. (Forootani et al., 2024). However, their approach focuses on inverse problems related to PDEs. Specifically, their QR-DEIM-based method is for parameter estimation, which begins with sampling points from data from the solution of a PDE with unknown parameters. In contrast, our approach is for solving the forward problem, which approximates the solution of a PDE - this divergence in focus results in fundamentally different algorithms.

1.2. Contributions

In this paper, we introduce a novel adaptive collocation point selection strategy for PINNs to solve forward problems related to PDEs. We compare the performance of our method to existing collocation point sampling techniques using the wave, Allen-Cahn equation, and Burgers' equation. Our results demonstrate that training a PINN with our approach achieves lower errors and convergence to lower test loss values in fewer iterations than current methods.

2. Methods

2.1. Background

ROM seeks to reduce the computational complexity and time of large-scale dynamical systems by finding lower-dimensional approximations that can replicate similar input-output responses. An area where ROM is particularly advantageous is high-dimensional systems of ordinary differential equations resulting from discretizing PDEs. Consider the following 1D nonlinear PDE of the form:

$$\frac{\partial u}{\partial t} = L(u) + F(u), \quad (1)$$

where $t \in [0, T]$ is the time variable with final time T , x is the spatial variable in some interval $[a, b]$, $u = u(x, t)$ is a scalar function satisfying (1), L is a linear spatial differential operator, and F is a nonlinear function of a scalar variable. A numerical discretization (i.e., finite difference) of (1) results in

$$\frac{d}{dt} \mathbf{u}(t) = \mathbf{A} \mathbf{u}(t) + \mathbf{F}(\mathbf{u}(t)), \quad (2)$$

where $\mathbf{u}(t) = [u_1(t), \dots, u_n(t)]^T \in \mathbb{R}^n$, the constant matrix $\mathbf{A} \in \mathbb{R}^{n \times n}$ is a discrete approximation of L , and \mathbf{F} is the nonlinear function F evaluated at $\mathbf{u}(t)$ component-wise, i.e. $\mathbf{F}(\mathbf{u}(t)) = [F(u_1(t)), \dots, F(u_n(t))]^T \in \mathbb{R}^n$.

Projection-based techniques are common in ROM (Lucia & Beran, 2003; Amsallem & Farhat, 2012; Wang et al., 2002). These methods construct a much smaller system of order $k \ll n$ that approximates the original system (i.e., (2)) using a subspace spanned by a reduced basis of dimension k in \mathbb{R}^n . In particular, let $\mathbf{V}_k \in \mathbb{R}^{n \times k}$ be a matrix whose columns form an orthonormal basis of this reduced space. By replacing $\mathbf{u}(t)$ with $\mathbf{V}_k \hat{\mathbf{u}}(t)$, $\hat{\mathbf{u}}(t) \in \mathbb{R}^k$, and projecting (2) onto the subspace spanned by the columns of \mathbf{V}_k , the reduced order system is of the form:

$$\frac{d}{dt} \hat{\mathbf{u}}(t) = \mathbf{V}_k^T \mathbf{A} \mathbf{V}_k \hat{\mathbf{u}}(t) + \mathbf{V}_k^T \mathbf{F}(\mathbf{V}_k \hat{\mathbf{u}}(t)). \quad (3)$$

The selection of a reduced order basis significantly influences the approximation's quality. Techniques for constructing reduced bases rely on the observation that the solution space for a given system is often embedded in a low-dimensional manifold. Consequently, the reduced basis is typically tailored to the specific problem. These methods create global basis functions derived from *snapshots* - discrete samples of trajectories from a set of different inputs and boundary conditions from the full-order system.

Proper orthogonal decomposition (POD) is a common method for constructing a low-dimensional approximation representation of a subspace in Hilbert space. Given a set of snapshots $Y = \{\mathbf{y}_1, \dots, \mathbf{y}_c\} \subset \mathbb{R}^n$ such that

$r = \text{rank}(\text{span}(Y))$, a POD basis of rank $k < r$ is the set of orthonormal vectors $\{\phi_1, \dots, \phi_k\}$ whose span best approximates the space Y . In other words, the vectors $\{\phi_1, \dots, \phi_k\}$ are the solution to

$$\min_{\phi_1, \dots, \phi_k} \sum_{i=1}^c \left\| \mathbf{y}_i - \sum_{j=1}^k (\mathbf{y}_j^T \phi_i) \phi_j \right\|_2^2. \quad (4)$$

It is well known that the solution (4) is given by the singular value decomposition (SVD) of the matrix $\mathbf{Y} = [\mathbf{y}_1, \dots, \mathbf{y}_r] \in \mathbb{R}^{n \times r}$, which we call the *snapshot matrix*. Let $\mathbf{Y} = \mathbf{V} \Sigma \mathbf{W}^T$ be the SVD decomposition of \mathbf{Y} , where $\mathbf{V} = [\mathbf{v}_1, \dots, \mathbf{v}_r] \in \mathbb{R}^{n \times r}$ and $\mathbf{W} = [\mathbf{w}_1, \dots, \mathbf{w}_r] \in \mathbb{R}^{c \times r}$ are orthogonal and $\Sigma = \text{diag}(\sigma_1, \dots, \sigma_r) \in \mathbb{R}^{r \times r}$ with $\sigma_1 \geq \sigma_2 \geq \dots \geq \sigma_r > 0$. The POD basis is then $\{\mathbf{v}_1, \dots, \mathbf{v}_k\}$.

Although POD has been shown to be successful in providing reduced-order models for numerous applications such as compressible flow (Bui-Thanh et al., 2003), fluid dynamics (Berkooz et al., 1993), and optimal control (Ravindran, 2000; Gubisch & Volkwein, 2017), it is not computationally efficient for systems with nonlinear terms (Kramer & Willcox, 2019). The discrete empirical interpolation method (DEIM) and later the QR-DEIM were introduced to address this computational bottleneck by efficiently approximating the nonlinear term $\mathbf{F}(\hat{\mathbf{u}}(t))$ (Chaturantabut & Sorensen, 2009; Drmac & Gugercin, 2016). A critical component of DEIM is the selection of interpolation points from snapshots of the nonlinear term. QR-DEIM is similar to DEIM but uses the QR decomposition of an orthonormal matrix (i.e., \mathbf{V}) with column pivoting to select the interpolation points.

2.2. Adaptive Collocation Strategy via the QR-DEIM Algorithm

We propose a strategy for adaptive collocation point selection in PINNs inspired by the QR-DEIM method. This approach involves constructing a snapshot matrix based on the residuals obtained from a set of snapshot points throughout the training process. Subsequently, we perform a singular value decomposition of this snapshot matrix and apply QR decomposition with column pivoting to select a subset of the snapshot points that we add to the training data. With this process, we can encode the residual dynamics between updates to the training set and use this information to select new collocation points.

Let $\mathcal{N}_\theta(x, t)$ be a neural network with trainable parameters θ , and let $\mathcal{T} = \{(x_i, t_i)\}_{i=1}^{N_{\text{train}}} \subset [a, b] \times [0, T]$ denote the set of collocation points used to train $\mathcal{N}_\theta(x, t)$ with some loss function \mathcal{L} . Additionally, let $\mathcal{S} = \{(x_i, t_i)\}_{i=1}^{N_{\text{snapshots}}} \subset [a, b] \times [0, T]$, with $\mathcal{T} \cap \mathcal{S} = \emptyset$, represent what we call snapshot points, which are sampled separately from the training points. Finally, let N_{budget} be the maximum number

of collocation points available for training.

Our collocation point selection strategy begins with $N_{\text{train}} \ll N_{\text{budget}}$ randomly sampled points. For a predefined period of P iterations, we compute the residuals $\mathbf{r}(\mathcal{S}) = [r((x_1, t_1)), \dots, r((x_{N_{\text{snapshots}}}, t_{N_{\text{snapshots}}}))]^T \in \mathbb{R}^{N_{\text{snapshots}}}$ on the set of snapshot points and construct a snapshot matrix of the form $\mathbf{Y} = [\mathbf{r}_1(\mathcal{S}), \dots, \mathbf{r}_P(\mathcal{S})] \in \mathbb{R}^{N_{\text{snapshots}} \times P}$, where $\mathbf{r}_i(\mathcal{S})$ are the residuals on the set of snapshot points at the i -th snapshot iteration. At the end of each period, we compute the SVD of \mathbf{Y} as $\mathbf{Y} = \mathbf{V}\Sigma\mathbf{W}^T$. Let $\varepsilon > 0$ be a user-defined threshold. The singular values in Σ represent the significance of their corresponding modes in the residual snapshot matrix. To best capture these dominant features in the error dynamics, we select the first N_{pivots} columns of \mathbf{V} , which correspond to singular values greater than or equal to ε . This selection forms the reduced matrix $\hat{\mathbf{V}} \in \mathbb{R}^{N_{\text{snapshots}} \times N_{\text{pivots}}}$.

The next step in this process is to apply QR decomposition with column pivoting to $\hat{\mathbf{V}}^T$. Recall that the pivoting matrix $\Pi \in \{0, 1\}^{N_{\text{snapshots}} \times N_{\text{snapshots}}}$ is a permutation matrix, where each column contains exactly one non-zero entry (i.e., 1). We select the points from \mathcal{S} that correspond to the row indices of the non-zero entries in the first N_{pivots} columns of Π . This selection yields N_{pivots} new points to add to our training set \mathcal{T} .

The final step in this update is to resample our snapshot points \mathcal{S} . We resample these points to ensure continued exploration of the domain, which helps to prevent bias toward specific regions and allows us to capture a broader range of error dynamics. Furthermore, this resampling helps maintain the size of $N_{\text{snapshots}}$ at a manageable level, which keeps the computational cost of computing the SVD and QR decomposition within reasonable limits. This process continues until we reach our point budget or a maximum number of iterations.

Throughout our sampling strategy, we also monitor the value of N_{pivots} and lower the threshold ε by an order of magnitude if N_{pivots} falls below a minimum threshold. This adjustment of ε takes into account changes in the magnitude of the residuals as the network becomes more accurate.

The complete collocation point selection strategy is detailed in Algorithm 1.

2.3. Training & Testing Protocols

To evaluate the effectiveness of our proposed collocation point sampling strategy, we compare its performance against three other methods: uniform random sampling (non-adaptive), greedy adaptive residual-based refinement sampling (Lu et al., 2021a), and distribution-based adaptive refinement sampling using the RAD method in (Wu et al., 2023). For the distribution-based method, we construct the

PDF as

$$p((x, t)) \propto \frac{r((x, t))^k}{\mathbb{E}[r((x, t))^k]} + c, \quad (5)$$

where c and k are hyperparameters. We choose the recommended default values $c = k = 1$.

We use a maximum of 500, 1,000, and 2,000 points for the wave, Allen-Cahn, and Burgers' equations, respectively. All of the adaptive methods begin with 100 initial training points. For the greedy refinement strategy, we sample the point with the highest residual from a random pool of 10,000 points every five iterations. For the distribution-based strategy, we sample points from a random pool of 10,000 points every 1,000 iterations. In the case of the wave equation, this sample size is 100 points. For the Allen-Cahn and Burgers' equations, we sample 250 points. For our QR-DEIM-based approach, the snapshot set size is 2,000 points, with a snapshot period of 1,000 iterations. Additionally, we start with an initial singular value threshold of 10^{-1} and reduce this threshold by an order of magnitude if fewer than 25 points are selected. We continue this process until we reach a minimum threshold value of 10^{-3} .

For all experiments, we use a feedforward neural network with five hidden layers and 64 hidden units per hidden layer. We use the tanh activation function between each layer. The output of each network is modified to strongly enforce the initial and boundary conditions for each example problem. We use the Adam optimizer with a learning rate of 10^{-3} . Our loss function is the mean squared error of the residual on the training set. All networks use a validation set consisting of 10,000 randomly sampled points, and we save the weights of each model that result in the lowest validation loss.

To evaluate the accuracy of our solutions, we employ the relative ℓ_2 and ℓ_∞ errors, defined as $\sqrt{\frac{\sum_i (\mathbf{u}_i - \tilde{\mathbf{u}}_i)^2}{\sum_i \mathbf{u}_i^2}}$ and $\frac{\max_i |\mathbf{u}_i - \tilde{\mathbf{u}}_i|}{\max_i |\mathbf{u}_i|}$, respectively, where \mathbf{u} and $\tilde{\mathbf{u}}$ are the true and predicted solutions. Because all the collocation point methods we assess are stochastic, we test each method on every example 100 times and report the mean and standard deviation for each metric.

All of our models and experiments are implemented in Python using PyTorch (2.5.1). We use an Nvidia H100 GPU to train our models. All the code necessary to reproduce our results is available at <https://github.com/accelaya/qr-deim-collocation>.

3. Results

In this section, we assess the accuracy of the sampling methods described in Sections 1.1 and 2.2 using the training and testing protocols outlined in Section 2.3 on the wave, Allen-Cahn, and Burgers' equations.

Algorithm 1 Adaptive Collocation Point Selection Using QR-DEIM

Input: Snapshot period P , snapshot set size $N_{\text{snapshots}}$, initial training set size N_{train} , singular value threshold ε , minimum singular value threshold ε_{min} , point budget N_{budget} , maximum iterations M , minimum number of update points m .

```

1:  $k \leftarrow 0$  ▷ Iteration counter.
2: Initialize neural network  $\mathcal{N}_\theta$ 
3: Randomly sample training data:  $\mathcal{T} \leftarrow \{(x_i, t_i)\}_{i=1}^{N_{\text{train}}}$ 
4: Randomly sample snapshot points:  $\mathcal{S} \leftarrow \{(x_i, t_i)\}_{i=1}^{N_{\text{snapshots}}}$ 
5: while  $k < M$  do ▷ Start training.
6:    $z \leftarrow k \bmod P$  ▷ Snapshot counter.
7:   Compute loss:  $\ell \leftarrow \mathcal{L}(\mathcal{N}_\theta(\mathcal{T}))$ .
8:   Update  $\theta$  via backpropagation with  $\ell$ .
9:   while  $N_{\text{train}} < N_{\text{budget}}$  do
10:    Update snapshot matrix:  $\mathbf{Y}[:, z+1] \leftarrow \mathbf{r}_{z+1}(\mathcal{S})$ . ▷ Compute residuals on snapshot points.
11:    if  $z = 0$  and  $k > 0$  then ▷ Update training set every  $P$  iterations.
12:      Compute SVD of snapshot matrix:  $\mathbf{Y} = \mathbf{V}\Sigma\mathbf{W}^T$ .
13:       $N_{\text{pivots}} \leftarrow |\{\Sigma_{ii} \geq \varepsilon : i = 1, \dots, P\}|$  ▷ Get number of update/pivot points.
14:      if  $N_{\text{pivots}} < m$  then ▷ Update  $\varepsilon$  if  $N_{\text{pivots}}$  is too low.
15:         $\varepsilon \leftarrow \max\{\varepsilon \times 10^{-1}, \varepsilon_{\text{min}}\}$  ▷ Put a floor on  $\varepsilon$ .
16:      end if
17:       $\hat{\mathbf{V}} \leftarrow \mathbf{V}[:, 1 : N_{\text{pivots}}]^T$  ▷ Only use first  $N_{\text{pivots}}$  columns of  $\mathbf{V}$ .
18:      Compute QR:  $\hat{\mathbf{V}} = \mathbf{Q}(\mathbf{R} \quad \mathbf{0})\Pi^T$ .
19:      Get indices:  $\mathcal{I} \leftarrow \{i : \Pi[:, 1 : N_{\text{pivots}}]_{ij} = 1\}$  ▷ Get indices of points in  $\mathcal{S}$  for updating  $\mathcal{T}$ .
20:      Update training data:  $\mathcal{T} \leftarrow \mathcal{T} \cup \{(x_i, t_i) \in \mathcal{S} : i \in \mathcal{I}\}$ .
21:      Re-sample snapshots:  $\mathcal{S} \leftarrow \{(x_i, t_i)\}_{i=1}^{N_{\text{snapshots}}}$ 
22:    end if
23:  end while
24:   $k \leftarrow k + 1$  ▷ Update iteration counter.
25: end while
    
```

3.1. Wave Equation

We begin by examining the wave equation stated below:

$$\begin{aligned} \frac{\partial^2 u}{\partial t^2} &= c^2 \frac{\partial^2 u}{\partial x^2}, \quad (x, t) \in (-1, 1) \times (0, 1] \\ \frac{\partial u}{\partial t} &= 0, \quad (x, t) \in [-1, 1] \times \{0\} \\ u(-1, t) &= u(1, t) = 0, \quad t \in [0, 1] \\ u(x, 0) &= \sin(\pi x), \quad x \in [-1, 1]. \end{aligned}$$

The exact solution is given by $u(x, t) = \sin(\pi x) \cos(c\pi t)$. In this example, we set the wave speed, denoted by c , to 2. Table 1 presents the mean and standard deviation of the relative ℓ_2 and ℓ_∞ errors for the wave equation using various collocation point sampling methods. Here, we see that our QR-DEIM-based approach demonstrates the lowest mean errors and variances for both norms. Figure 2 shows predictions, the difference between true and predicted solutions, and the collocation points selected by each sampling method. The horizontal and vertical axes represent the time and space variables, respectively. Figure 5 (left) shows the average test loss curve for each sampling method for this example.

Table 1. Mean and standard deviation of the relative ℓ_2 and ℓ_∞ errors for the wave equation using different collocation point sampling methods.

Method	Rel. ℓ_2 Error	Rel. ℓ_∞ Error
Uniform Random	1.85e-02 (3.64e-02)	2.47e-02 (4.87e-02)
Greedy	1.62e-02 (7.11e-03)	2.29e-02 (8.76e-03)
Distribution-based	1.12e-02 (9.61e-03)	1.57e-02 (1.29e-02)
QR-DEIM	7.04e-03 (5.31e-03)	1.02e-02 (8.30e-03)

3.2. Allen-Cahn Equation

To test our approach on a nonlinear PDE, we consider the Allen-Cahn equation stated below:

$$\begin{aligned} \frac{\partial u}{\partial t} &= \alpha \frac{\partial^2 u}{\partial x^2} + \frac{1}{\beta^2} f(u), \quad (x, t) \in (-1, 1) \times (0, 1] \\ u(-1, t) &= u(1, t) = -1, \quad t \in [0, 1] \\ u(x, 0) &= x^2 \cos(\pi x), \quad x \in [-1, 1]. \end{aligned}$$

In this case, we set the diffusion coefficient α to 10^{-3} , the value of β to $5^{-1/2}$, and the function $f(u) = u^3 - u$. Table 2 presents the mean and standard deviation of the relative

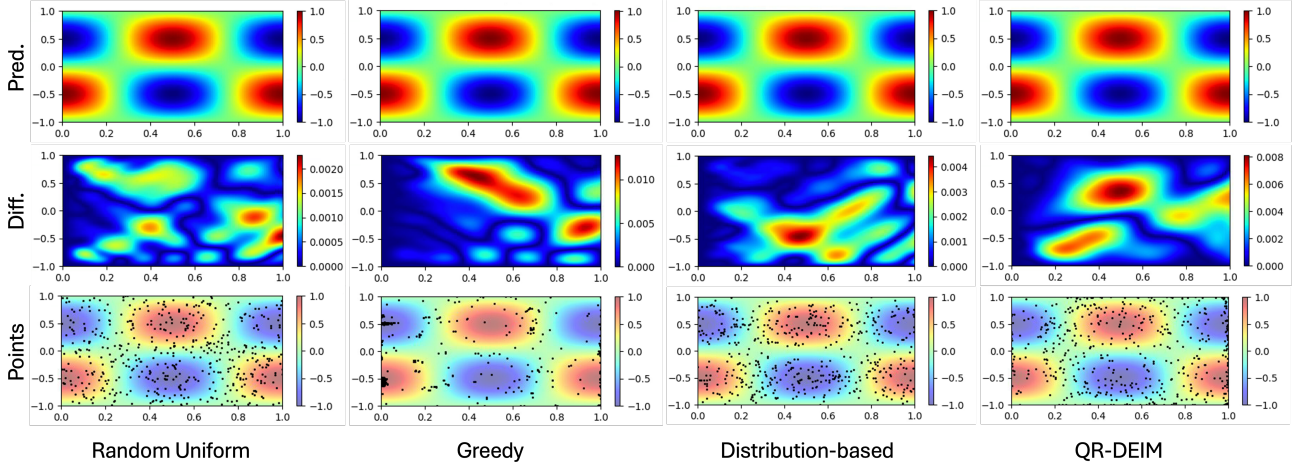


Figure 2. From top to bottom, predictions, absolute value of pointwise error, and collocation points for the wave equation using uniform random, greedy, distribution-based, and QR-DEIM-based collocation point sampling.

ℓ_2 and ℓ_∞ errors for the Allen-Cahn equation using various collocation point sampling methods. Like with the wave equation, our QR-DEIM-based approach demonstrates consistently lower errors in both norms vs. the other collocation point sampling methods. Figure 3 shows predictions, the difference between true and predicted solutions, and the collocation points selected by each sampling method. Figure 5 (center) shows the average test loss curve for each sampling method for this example.

Table 2. Mean and standard deviation of the relative ℓ_2 and ℓ_∞ errors for the Allen-Cahn equation using different collocation point sampling methods.

Method	Rel. ℓ_2 Error	Rel. ℓ_∞ Error
Uniform Random	2.71e-01 (8.66e-02)	9.78e-01 (2.74e-01)
Greedy	6.53e-01 (2.20e-01)	1.77e+01 (3.49e-01)
Distribution-based	1.64e-01 (9.86e-02)	7.57e-01 (3.35e-01)
QR-DEIM	7.08e-02 (5.24e-02)	4.35e-01 (1.53e-01)

3.3. Burgers' Equation

Finally, we consider Burgers' equation given by

$$\begin{aligned} \frac{\partial u}{\partial t} &= \nu \frac{\partial^2 u}{\partial x^2} - u \frac{\partial u}{\partial x}, \quad (x, t) \in (-1, 1) \times (0, 1] \\ u(-1, t) &= u(1, t) = 0, \quad t \in [0, 1] \\ u(x, 0) &= -\sin(\pi x), \quad x \in [-1, 1], \end{aligned}$$

where we set the viscosity term ν equal to $0.01/\pi$. This example allows us to see how our method behaves in the presence of a shock or strong front in the solution. Table 3 presents the mean and standard deviation of the relative ℓ_2 and ℓ_∞ errors for Burgers' equation when using various collocation point sampling methods. Our QR-DEIM-based

approach shows an order of magnitude improvement in the relative ℓ_2 error compared to other sampling methods, as well as a similar improvement in the relative ℓ_∞ error when compared to uniform sampling and distribution-based strategies. Figure 4 shows predictions, the difference between true and predicted solutions, and the collocation points selected by each sampling method. Figure 5 (right) shows the average test loss curve for each sampling method for this example.

Table 3. Mean and standard deviation of the relative ℓ_2 and ℓ_∞ errors for Burgers' equation using different collocation point sampling methods.

Method	Rel. ℓ_2 Error	Rel. ℓ_∞ Error
Uniform Random	2.69e-01 (1.42e-01)	1.71e+01 (4.38e-01)
Greedy	1.17e-01 (1.18e-01)	8.45e-01 (7.52e-01)
Distribution-based	2.31e-01 (9.34e-02)	1.76e+01 (2.33e-01)
QR-DEIM	3.75e-02 (2.22e-02)	2.63e-01 (1.81e-01)

4. Discussion

The results in Section 3 indicate that our proposed QR-DEIM-based collocation point selection strategy improves the accuracy of PINNs. Indeed, for each of the benchmark problems, our method consistently outperforms existing collocation point sampling techniques, achieving large improvements in the relative ℓ_2 error. This higher accuracy is particularly apparent in more complex problems like the Allen-Cahn and Burgers' equation, where the solutions exhibit considerably more complex behavior than the wave equation. These results highlight the ability of our method to adaptively allocate collocation points to regions of high solution complexity, ensuring that challenging features, such as

PINN Collocation Points via QR-DEIM

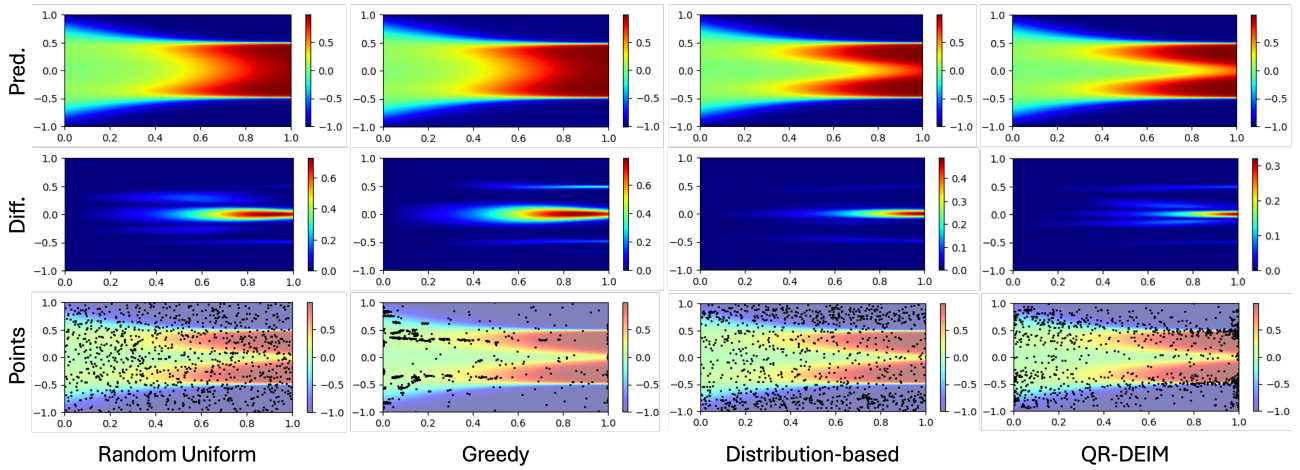


Figure 3. From top to bottom, predictions, absolute value of pointwise error, and collocation points for the Allen-Cahn equation using uniform random, greedy, distribution-based, and QR-DEIM-based collocation point sampling.

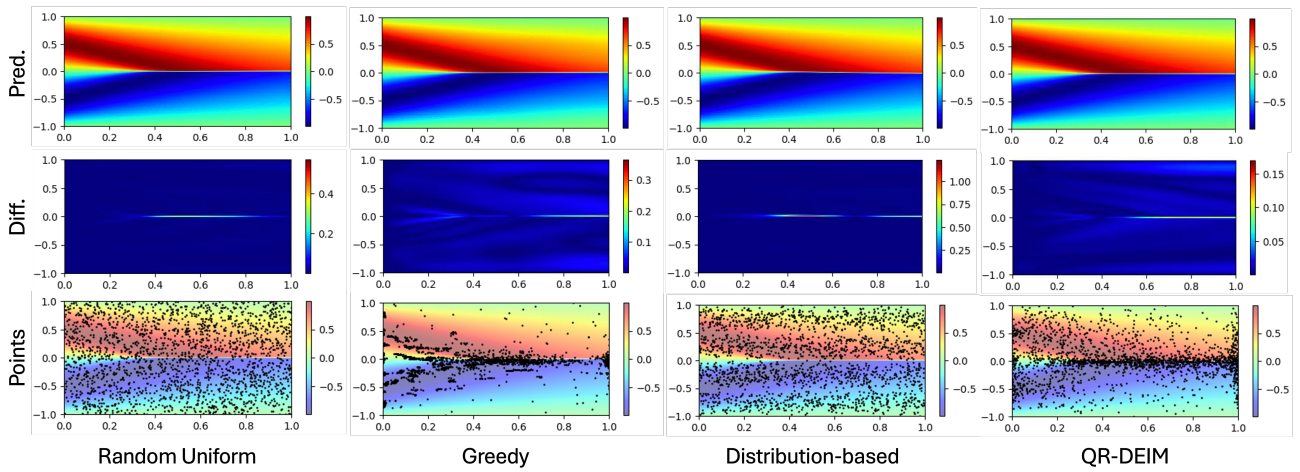


Figure 4. From top to bottom, predictions, absolute value of pointwise error, and collocation points for Burgers' equation using uniform random, greedy, distribution-based, and QR-DEIM-based collocation point sampling.

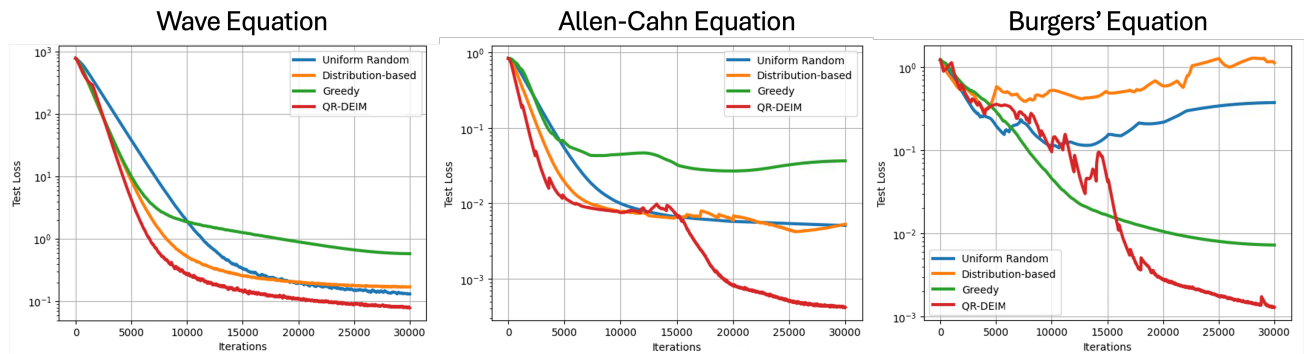


Figure 5. Average test loss curves over 100 simulations for uniform random, greedy, distribution-based, and QR-DEIM-based collocation point sampling for the wave (left), Allen-Cahn (center), and Burgers' (right) equations.

sharp gradients or localized phenomena, are well-resolved. Furthermore, the lower variability of results across multiple problems highlights the robustness of the QR-DEIM-based strategy.

The bottom rows of Figures 2, 3, and 4 illustrate the collocation points chosen by each method. The corresponding loss curves (see Figure 5) further emphasize the advantages of our method, showing rapid convergence and consistently lower test losses compared to other sampling strategies across all benchmark problems. This convergence to lower test losses demonstrates that the QR-DEIM-based approach not only improves point selection but also directly impacts the optimization process and final solution accuracy.

In the case of the wave equation, we observe that the sampling strategies tend to select distributions of collocation points that roughly look similar, except for the points obtained with the greedy method. A subtle distinction between our proposed method and the alternative sampling techniques is its tendency to select more points closer to the final time (i.e., $t = 1$). This clustering toward the end of the time interval is likely beneficial for training PINNs to address time-dependent problems, as the error in a PINN solution for such problems tends to increase significantly with longer simulation times (Chen et al., 2024).

The differences between the sets of collocation points become apparent with the Allen-Cahn and Burgers' equations. Like with the wave equation, our proposed method tends to select more points near the end of the time interval for both of these cases. For the Allen-Cahn equation, we see that our QR-DEIM-based approach also tends to cluster points near the phase boundaries, which have high gradients. On the other hand, the distribution-based sampling strategy tends to select points in the regions between the spatial endpoints (i.e., $x = -1$ and $x = 1$) and the phase boundary, which are relatively flat. The greedy approach does not do well with the Allen-Cahn equation, and this method chooses points in tight clusters toward the beginning of the time interval, neglecting important regions with more complex behavior.

Burgers' equation has a shock that develops at the point $x = 0$. This shock is where the largest errors occur for PINNs trained using each sampling method. However, our proposed sampling method achieves the lowest errors in this scenario, with the distribution of sampling points concentrated around the shock location. We hypothesize that this concentration ensures that the model trained using this distribution of collocation points better captures the steep gradients associated with the shock. In addition, the ability of our method to maintain accuracy away from the shock highlights its capacity to balance local accuracy and global consistency, addressing challenges presented by nonlinear dynamics.

In contrast to the Allen-Cahn equation, the greedy sampling method yields the second lowest errors and also demonstrates a significant clustering of points at the shock location. Nonetheless, the greedy approach takes this clustering to an extreme, almost entirely neglecting regions away from the shock. This neglect likely limits the model's ability to represent the solution globally, which can be critical for applications where the solution behavior across the entire domain is important. Conversely, the distribution-based sampling method does not exhibit strong clustering around the shock; instead, it selects what appears to be loose bands of points traveling along the time axis. This selection results in results similar to those of models trained with uniformly random sampled points.

Our method strikes a balance between the greedy and distribution-based sampling methods for Burgers' equation - it clusters points around the shock location while still accounting for other regions. This balance not only minimizes errors near the shock but also allows the model to achieve lower overall errors, demonstrating the versatility and adaptability of the QR-DEIM-based collocation point selection strategy across varying problem complexities. These findings suggest that our method is well-suited for problems where sharp gradients coexist with smoother regions, as it can dynamically allocate new collocation points to where they are needed most.

While our approach shows promise, further testing is needed on different problems. Assessing the performance of the QR-DEIM-based collocation point selection strategy on a broader range of benchmark problems, including higher-dimensional or coupled systems, will help evaluate its generalizability. Additionally, integrating this method with other advancements in PINNs, like the loss functions and architectures described in Section 1.1, could enhance its effectiveness. Future work could also explore theoretical guarantees for the performance of QR-DEIM in selecting collocation points and their effect on training PINNs.

5. Conclusions

When tested on a range of benchmark problems, our approach achieved a significant reduction in the relative ℓ_2 error and convergence to lower test loss values in fewer iterations vs. current collocation point sampling methods. Future work will include further validation of our method on more complex problems, combining it with recent advancements like improved loss functions and architectures for PINNs, and investigating theoretical aspects of our collocation point sampling technique. Overall, our results provide a strong foundation for the continued development and application of advanced collocation point selection strategies in PINNs.

References

- Amsallem, D. and Farhat, C. Stabilization of projection-based reduced-order models. *International Journal for Numerical Methods in Engineering*, 91(4):359–377, 2012.
- Berkooz, G., Holmes, P., and Lumley, J. L. The proper orthogonal decomposition in the analysis of turbulent flows. *Annual review of fluid mechanics*, 25(1):539–575, 1993.
- Bui-Thanh, T., Damodaran, M., and Willcox, K. Proper orthogonal decomposition extensions for parametric applications in compressible aerodynamics. In *21st AIAA applied aerodynamics conference*, pp. 4213, 2003.
- Cai, S., Mao, Z., Wang, Z., Yin, M., and Karniadakis, G. E. Physics-informed neural networks (PINNs) for fluid mechanics: A review. *Acta Mechanica Sinica*, 37(12):1727–1738, 2021.
- Chaturantabut, S. and Sorensen, D. C. Discrete empirical interpolation for nonlinear model reduction. In *Proceedings of the 48th IEEE Conference on Decision and Control (CDC) held jointly with 2009 28th Chinese Control Conference*, pp. 4316–4321. IEEE, 2009.
- Chaturantabut, S. and Sorensen, D. C. Nonlinear model reduction via discrete empirical interpolation. *SIAM Journal on Scientific Computing*, 32(5):2737–2764, 2010.
- Chen, Z., Lai, S.-K., and Yang, Z. AT-PINN: Advanced time-marching physics-informed neural network for structural vibration analysis. *Thin-Walled Structures*, 196:111423, 2024.
- Degen, D., Cacace, M., and Wellmann, F. 3D multi-physics uncertainty quantification using physics-based machine learning. *Scientific Reports*, 12(1):17491, 2022.
- Drmac, Z. and Gugercin, S. A new selection operator for the discrete empirical interpolation method—improved a priori error bound and extensions. *SIAM Journal on Scientific Computing*, 38(2):A631–A648, 2016.
- Forootani, A., Kapadia, H., Chellappa, S., Goyal, P., and Benner, P. GS-PINN: Greedy sampling for parameter estimation in partial differential equations. *arXiv preprint arXiv:2405.08537*, 2024.
- Gao, W. and Wang, C. Active learning based sampling for high-dimensional nonlinear partial differential equations. *Journal of Computational Physics*, 475:111848, 2023.
- Gubisch, M. and Volkwein, S. Proper orthogonal decomposition for linear-quadratic optimal control. *Model reduction and approximation: theory and algorithms*, 15(1), 2017.
- Hanna, J. M., Aguado, J. V., Comas-Cardona, S., Askri, R., and Borzacchiello, D. Residual-based adaptivity for two-phase flow simulation in porous media using physics-informed neural networks. *Computer Methods in Applied Mechanics and Engineering*, 396:115100, 2022.
- Karniadakis, G. E., Kevrekidis, I. G., Lu, L., Perdikaris, P., Wang, S., and Yang, L. Physics-informed machine learning. *Nature Reviews Physics*, 3(6):422–440, 2021.
- Kramer, B. and Willcox, K. E. Nonlinear model order reduction via lifting transformations and proper orthogonal decomposition. *AIAA Journal*, 57(6):2297–2307, 2019.
- Lu, L., Meng, X., Mao, Z., and Karniadakis, G. E. DeepXDE: A deep learning library for solving differential equations. *SIAM review*, 63(1):208–228, 2021a.
- Lu, L., Pestourie, R., Yao, W., Wang, Z., Verdugo, F., and Johnson, S. G. Physics-informed neural networks with hard constraints for inverse design. *SIAM Journal on Scientific Computing*, 43(6):B1105–B1132, 2021b.
- Lucia, D. J. and Beran, P. S. Projection methods for reduced order models of compressible flows. *Journal of Computational Physics*, 188(1):252–280, 2003.
- Nabian, M. A., Gladstone, R. J., and Meidani, H. Efficient training of physics-informed neural networks via importance sampling. *Computer-Aided Civil and Infrastructure Engineering*, 36(8):962–977, 2021.
- Pang, G., Lu, L., and Karniadakis, G. E. fPINNs: Fractional physics-informed neural networks. *SIAM Journal on Scientific Computing*, 41(4):A2603–A2626, 2019.
- Psaros, A. F., Kawaguchi, K., and Karniadakis, G. E. Meta-learning PINN loss functions. *Journal of computational physics*, 458:111121, 2022.
- Raissi, M., Perdikaris, P., and Karniadakis, G. E. Physics-informed neural networks: A deep learning framework for solving forward and inverse problems involving nonlinear partial differential equations. *Journal of Computational physics*, 378:686–707, 2019.
- Ravindran, S. S. A reduced-order approach for optimal control of fluids using proper orthogonal decomposition. *International journal for numerical methods in fluids*, 34(5):425–448, 2000.
- Wang, J. M., Chu, C.-C., Yu, Q., and Kuh, E. S. On projection-based algorithms for model-order reduction of interconnects. *IEEE Transactions on Circuits and Systems I: Fundamental Theory and Applications*, 49(11):1563–1585, 2002.

- Wang, Y. and Zhong, L. NAS-PINN: neural architecture search-guided physics-informed neural network for solving PDEs. *Journal of Computational Physics*, 496: 112603, 2024.
- Wang, Y., Shi, L., Hu, X., Song, W., and Wang, L. Multiphysics-informed neural networks for coupled soil hydrothermal modeling. *Water Resources Research*, 59 (1):e2022WR031960, 2023.
- Wu, C., Zhu, M., Tan, Q., Kartha, Y., and Lu, L. A comprehensive study of non-adaptive and residual-based adaptive sampling for physics-informed neural networks. *Computer Methods in Applied Mechanics and Engineering*, 403:115671, 2023.
- Yazdani, A., Lu, L., Raissi, M., and Karniadakis, G. E. Systems biology informed deep learning for inferring parameters and hidden dynamics. *PLoS computational biology*, 16(11):e1007575, 2020.
- Yu, J., Lu, L., Meng, X., and Karniadakis, G. E. Gradient-enhanced physics-informed neural networks for forward and inverse PDE problems. *Computer Methods in Applied Mechanics and Engineering*, 393:114823, 2022.
- Zapf, B., Haubner, J., Kuchta, M., Ringstad, G., Eide, P. K., and Mardal, K.-A. Investigating molecular transport in the human brain from MRI with physics-informed neural networks. *Scientific Reports*, 12(1):15475, 2022.
- Zeng, S., Zhang, Z., and Zou, Q. Adaptive deep neural networks methods for high-dimensional partial differential equations. *Journal of Computational Physics*, 463: 111232, 2022.